Supplementary materials

Oxalamide based Fe(II)-MOFs as potential electrode modifiers for glucose detection

Panagiotis Oikonomopoulos [1]**, Varvara Pagkali** [2]**, Evangelia Kritikou** [2]**, Anthi Panara** [2]**, Marios G. Kostakis** [2]**, Nicolaos S. Thomaidis** [2]**, Thomais G. Tziotzi** [3]**, Anastasios Economou** [2]**, Christos Kokkinos** [2] **and Giannis S. Papaefstathiou** [1,*]

[1] Laboratory of Inorganic Chemistry, Department of Chemistry, National and Kapodistrian University of Athens, 15771 Athens, Greece

[2] Laboratory of Analytical Chemistry, Department of Chemistry, National and Kapodistrian University of Athens, 15771 Athens, Greece

[3] Department of Chemistry, University of Crete, Voutes 710 03, Herakleion, Greece

[*] Correspondence: gspapaef@chem.uoa.gr

Table S1. Crystal data and structure refinement for the two compounds.

Identification code	3D-Fe-MOF	2D-Fe-MOF
Empirical formula	$C_{18}H_{18}Fe_2N_2O_{15}$	$C_{18}H_{18}FeN_2O_{14}$
Formula weight	614.04	542.19
Temperature/K	293(2)	219.99
Crystal system	triclinic	monoclinic
Space group	P-1	$P2_1/n$
a/Å	9.872(11)	10.7010(3)
b/Å	9.893(9)	4.49550(10)
c/Å	10.889(13)	21.6669(6)
$\alpha/°$	77.72(4)	90
$\beta/°$	84.23(4)	94.7210(10)
$\gamma/°$	89.29(3)	90
Volume/Å³	1033.8(19)	1038.78(5)
Z	2	2
ρ_{calc}g/cm³	1.973	1.733
μ/mm⁻¹	12.099	6.591
F(000)	624.0	556.0
Crystal size/mm³	0.165 × 0.015 × 0.015	0.21 × 0.085 × 0.02
Radiation	$CuK\alpha$ (λ = 1.54178)	$CuK\alpha$ (λ = 1.54178)
2Θ range for data collection/°	8.352 to 129.976	8.188 to 136.79
Index ranges	-11 ≤ h ≤ 11, -11 ≤ k ≤ 11, -12 ≤ l ≤ 12	-10 ≤ h ≤ 12, -5 ≤ k ≤ 5, -26 ≤ l ≤ 26
Reflections collected	7679	9797
Independent reflections	3409 [R_{int} = 0.0653, R_{sigma} = 0.0860]	1899 [R_{int} = 0.0439, R_{sigma} = 0.0293]
Data/restraints/parameters	3409/2/355	1899/0/196
Goodness-of-fit on F²	1.071	1.061
Final R indexes [I>=2σ (I)]	R_1 = 0.0671, wR_2 = 0.1823	R_1 = 0.0312, wR_2 = 0.0876
Final R indexes [all data]	R_1 = 0.0907, wR_2 = 0.2034	R_1 = 0.0318, wR_2 = 0.0886
Largest diff. peak/hole / e Å⁻³	1.14/-0.95	0.54/-0.31
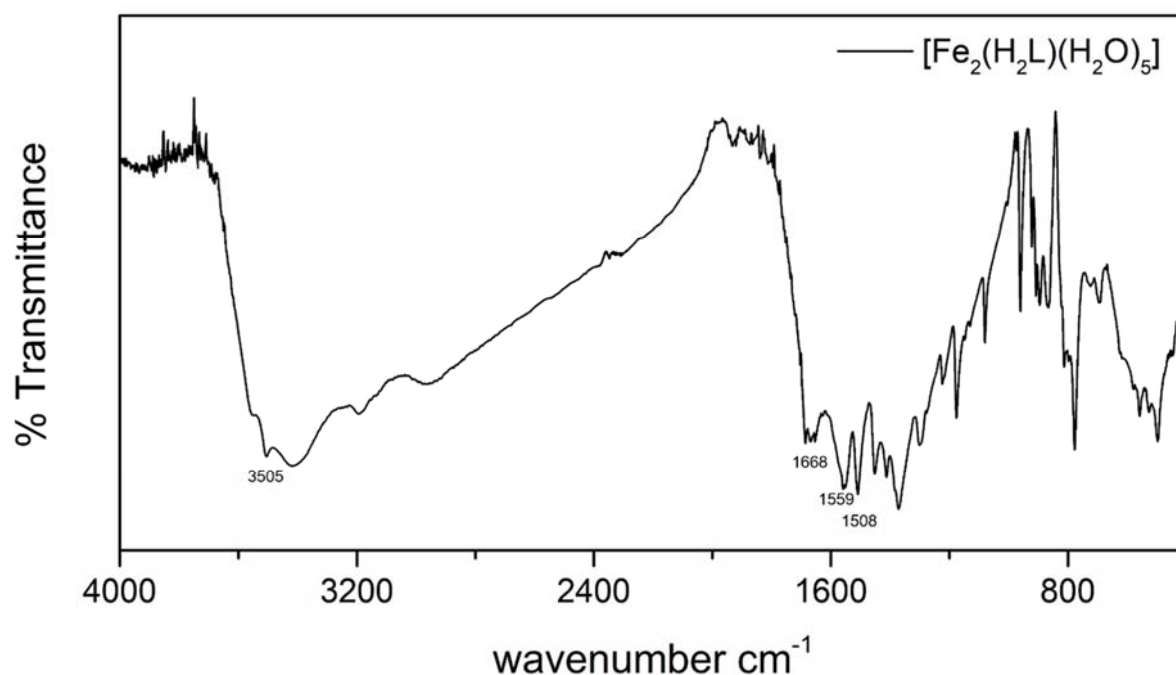
Figure S1. The IR spectra (KBr disc) of [Fe$_2$(H$_2$L)(H$_2$O)$_5$]. Free N-H vibration is observed at around 3505 cm^{-1}. C-N stretching vibration is found at 1301 cm^{-1}. The stretching vibrations ν(C=O) of the carbonyl group is observed at 1668 cm^{-1}. The peaks 1559 cm^{-1} and 1451 cm^{-1} are attributed to the asymmetric vibrations of the deprotonated carboxylates while at 1508 cm^{-1} and 1412 cm^{-1} to the respective symmetric vibrations. The stretch of the C=O of the carboxylate which is anticipated at around 1710 cm^{-1} is absent due to the tetra-deportation of the ligand.
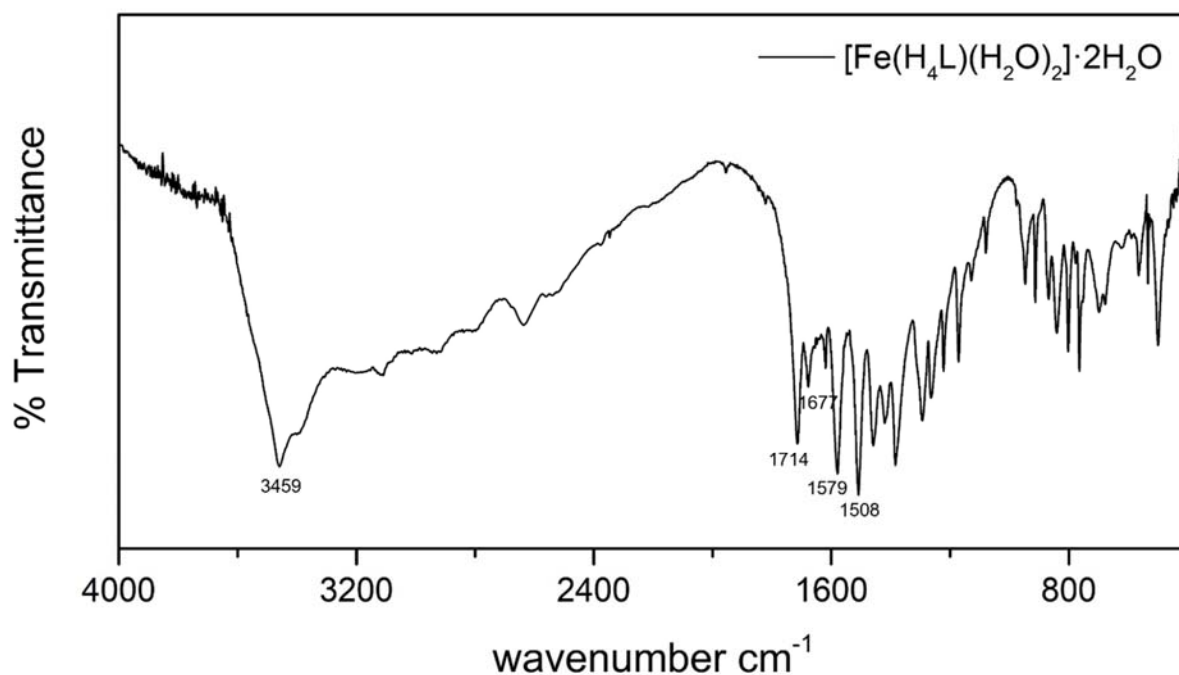
Figure S2. The IR spectra (KBr disc) of [Fe(H4L)(H2O)2]·2H2O. Free N-H absorption is observed at around 3459 cm-1. C-N stretching vibration is found at 1294 cm^{-1}. The stretching vibrations ν(C=O) of the carbonyl group is observed at 1677 cm^{-1}. The peaks 1579 cm^{-1} and 1458 cm^{-1} are attributed to the asymmetric vibrations of the deprotonated carboxylates while at 1508 cm^{-1} and 1420 cm^{-1} to the respective symmetric vibrations. Because of the deprotonation of the ligand (H4L^{-2}) the stretch of the C=O of the carboxylate can be observed at 1714 cm^{-1}.
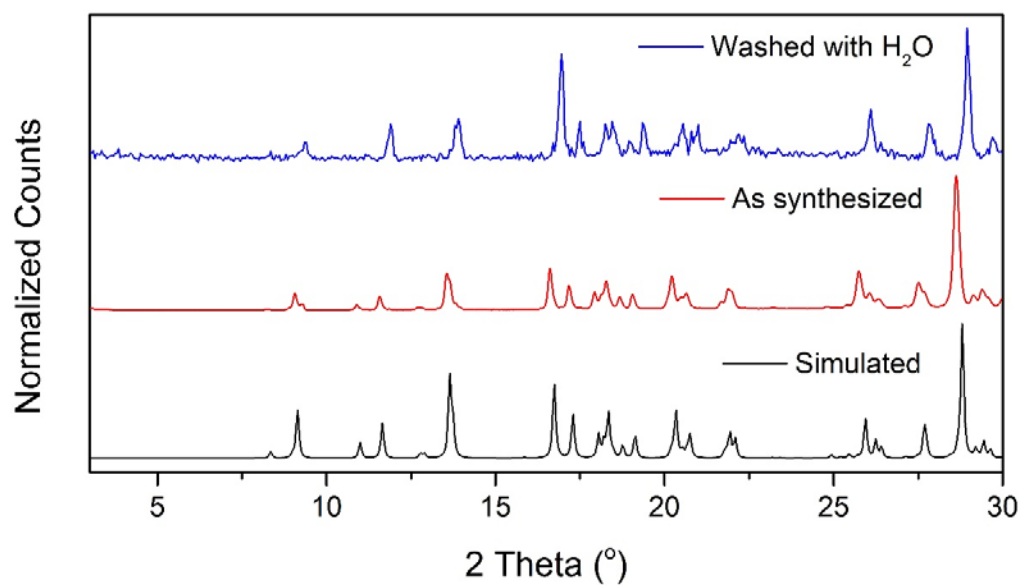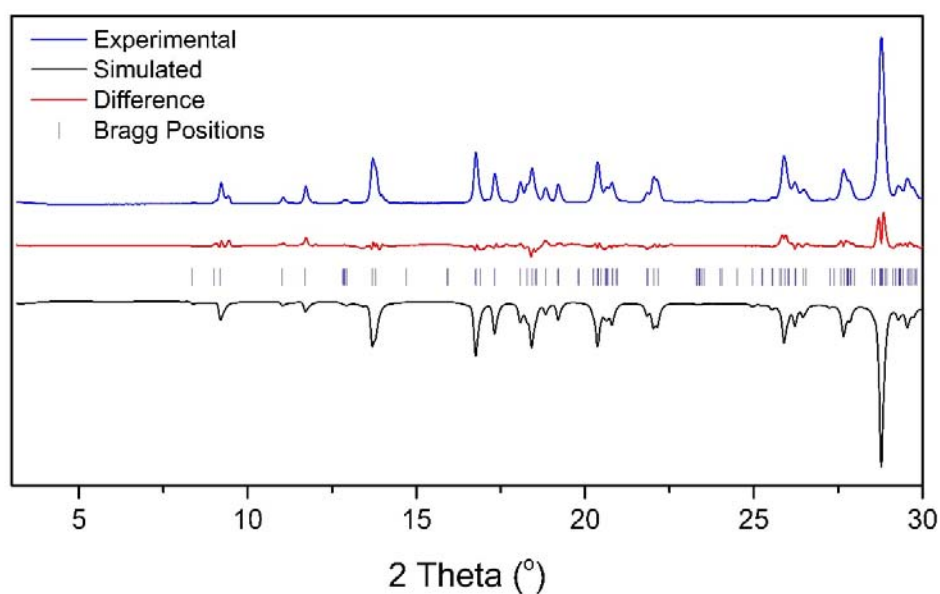
Figure S3. The PXRD patterns of $[Fe_2(H_2L)(H_2O)_5]$.

Figure S4. Le Bail refinement plot showing the experimental, simulated (reverted) and difference powder diffraction patterns of $[Fe_2(H_2L)(H_2O)_5]$. Vertical markers refer to the calculated positions of the Bragg reflections. Rp = 4.281, Rwp = 7.104, Weighting scheme: w=1.0/ycount, Profile function: Pearson VII.
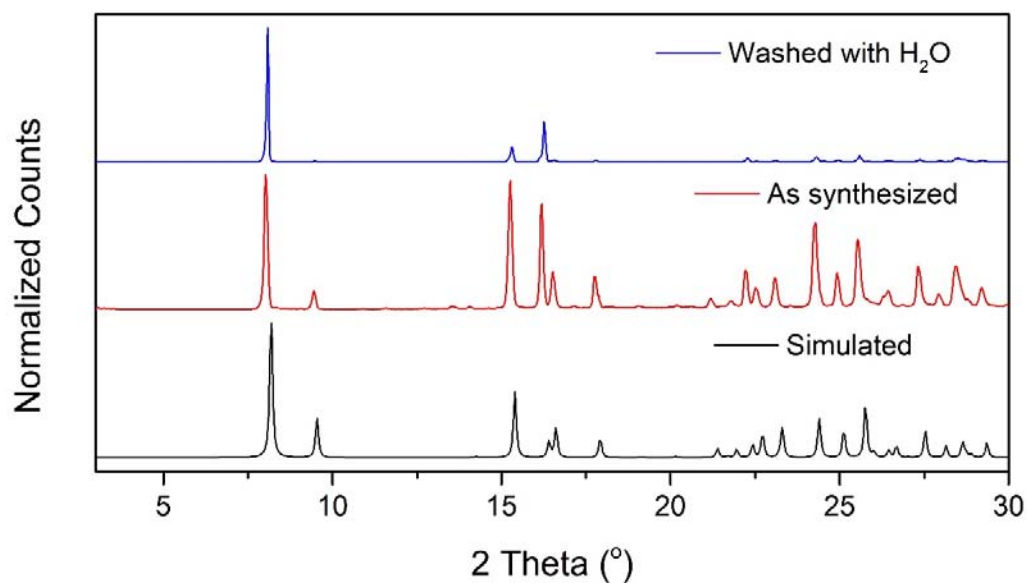
Figure S5. The PXRD patterns of $[Fe(H_4L)(H_2O)_2] \cdot 2H_2O$.

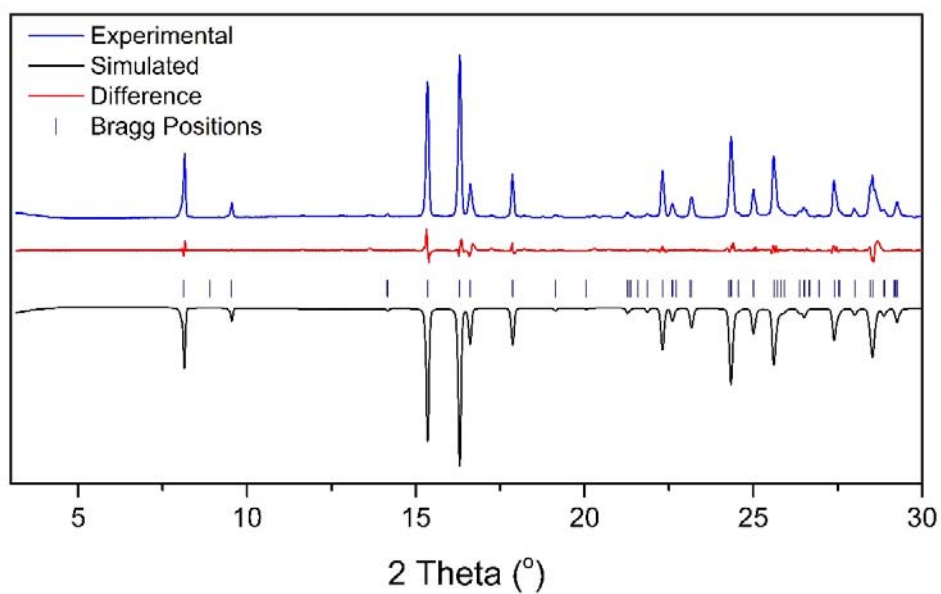**Figure S6**. Le Bail refinement plot showing the experimental, simulated (reverted) and difference powder diffraction patterns of $[Fe(H_4L)(H_2O)_2] \cdot 2H_2O$. Vertical markers refer to the calculated positions of the Bragg reflections. Rp = 6.038, Rwp = 7.153, Weighting scheme: w=1.0/ycount^2, Profile function: Pseudo-Voigt.
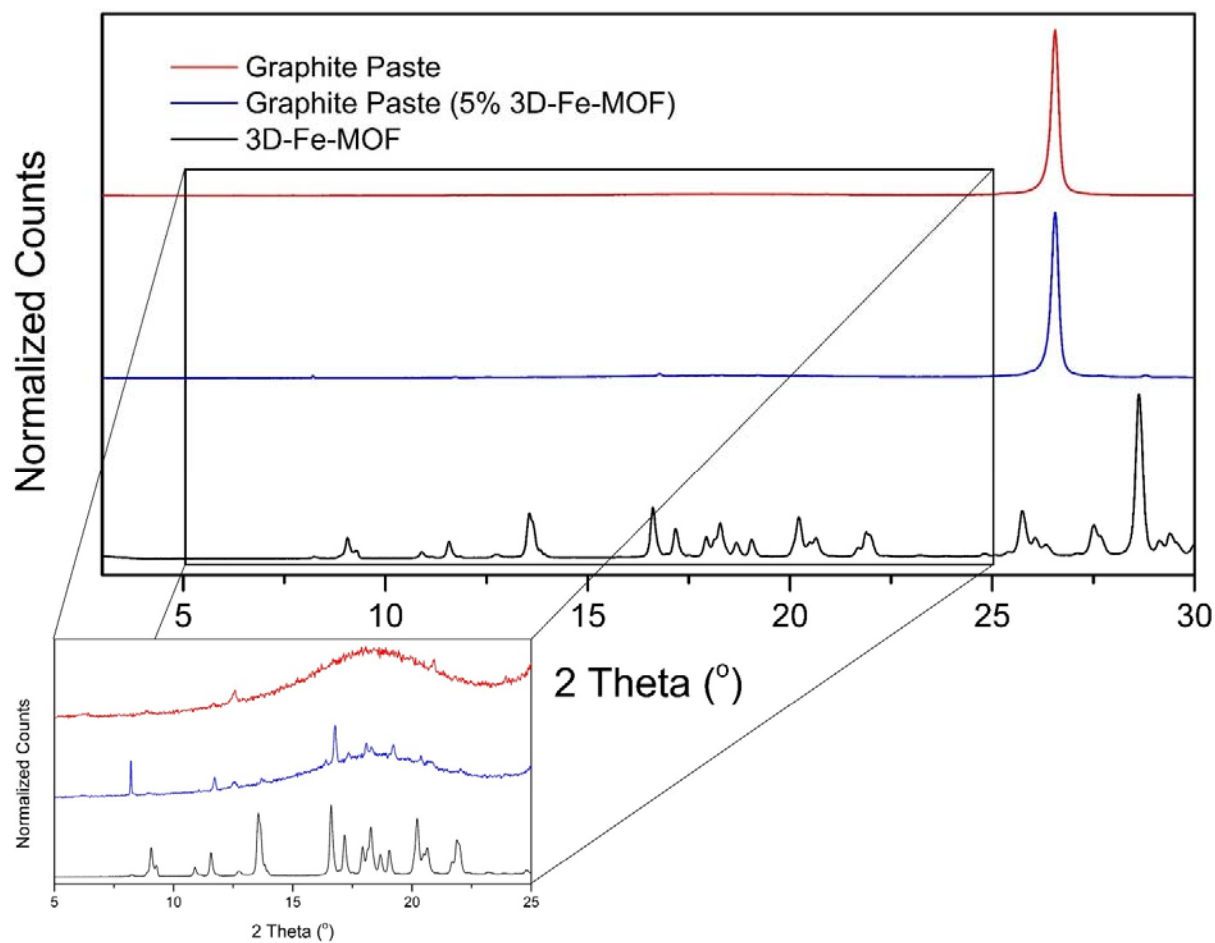
Figure S7. The PXRD patterns of the graphite paste (red line), of the $[Fe_2(H_2L)(H_2O)_5]$ (black line) and of the graphite paste with 5% of $[Fe_2(H_2L)(H_2O)_5]$ (blue line). Besides the low percentage of the MOF and the preferred orientation of the pattern, characteristic peaks of the MOF are visible in the pxrd of the enriched graphite paste.
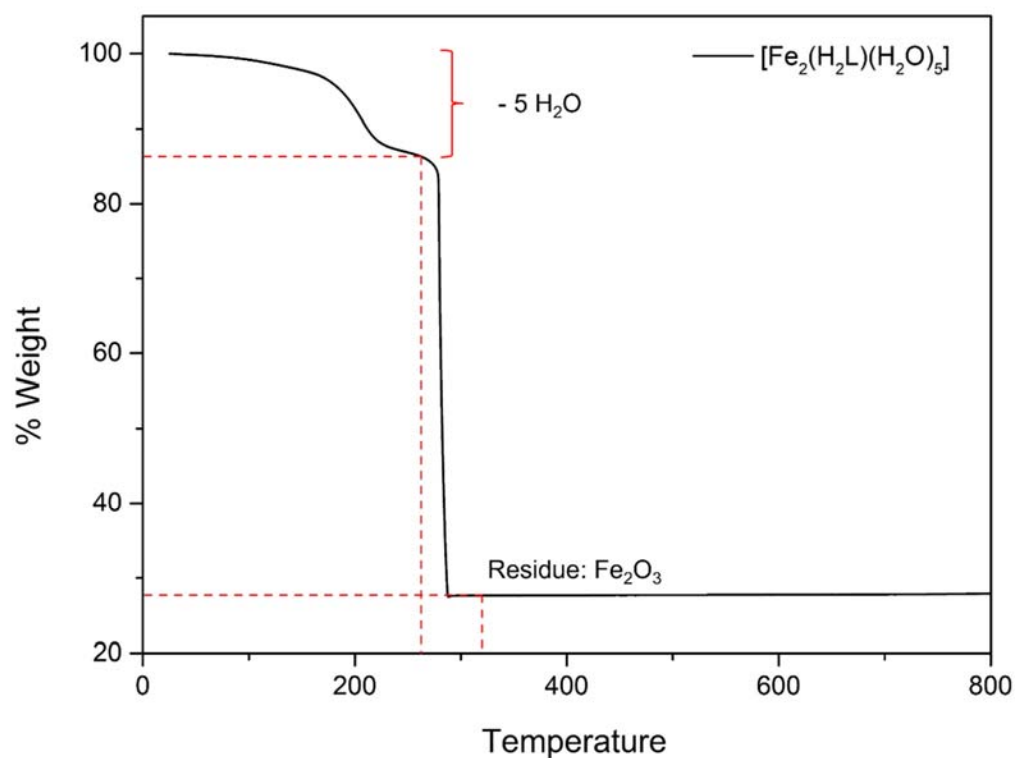
Figure S8. Thermogravimetric analysis reveals that [Fe$_2$(H$_2$L)(H$_2$O)$_5$] losses ~ 13.69% within 25 - 260 ° C temperature range which is very close to the theoretical value of the five coordinated H$_2$O molecules (theoretical value 14.65%). The residue above 360 °C is ~ 27.65% which corresponds to Fe$_2$O$_3$ (theoretical value 26.05%).
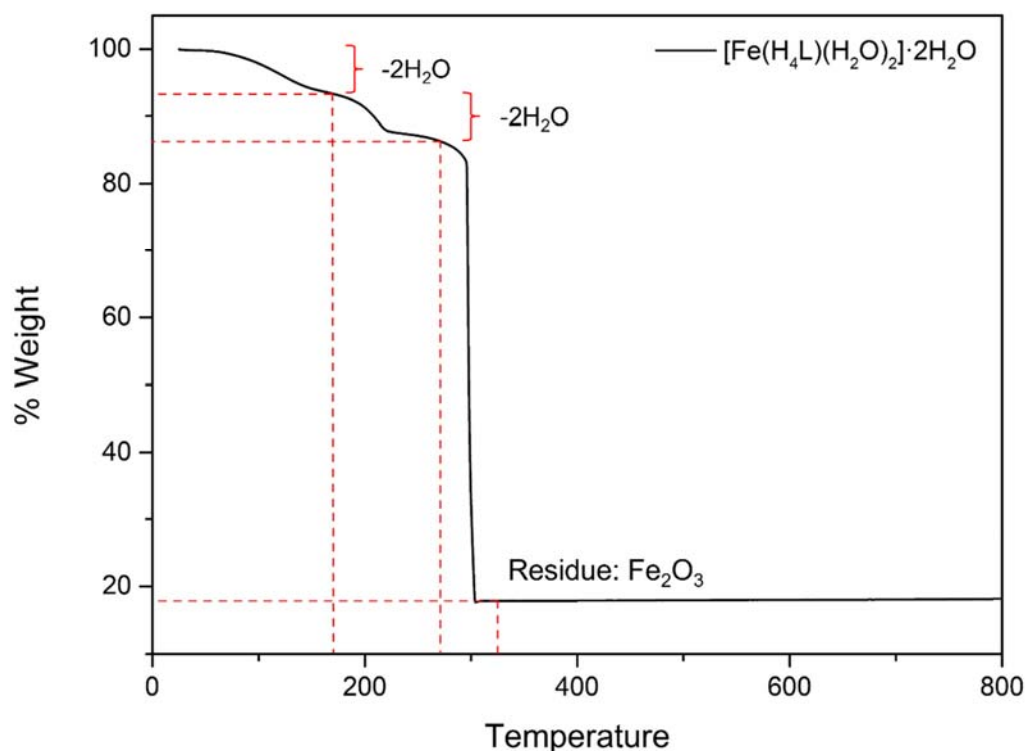
Figure S9. The Thermographic analysis of $[Fe(H_4L)(H_2O)_2] \cdot 2H_2O$. Thermogravimetric analysis reveals that $[Fe(H_4L)(H_2O)_2] \cdot 2H_2O$ losses ~ 6.45% within 25 - 170 °C temperature range which is very close to the theoretical value of the two H_2O molecules in the lattice (theoretical value 6.64%) followed by a loss of ~ 6.96% within the 170 – 260 °C that can be attributed to the loss of the two coordinated H_2O molecules (theoretical value 6.64%). The residue above 360 °C is ~ 17.83% which corresponds to Fe_2O_3 (theoretical value 20.06%).

Sorption studies

Chemicals and Reagents

All standards and reagents used, were of high-purity grade (>95%). Glucose and Glucose-[13]C (internal standard-IS) were purchased from Sigma-Aldrich (Stenheim, Germany). Acetonitrile (ACN) (LC-MS grade) and hydrochloric acid were acquired from Merck (Darmstadt, Germany), while ammonia hydroxide solution (25%) (NH_4OH) was obtained from Carlo Ebra (Val-de-Reuil, France). Distilled water was provided by a Milli-Q purification apparatus (Millipore Direct-Q UV, Bedford, MA, USA). Regenerated cellulose syringe filters (RC filters, pore size 0.2 μm, diameter 15 mm) were obtained from Macherey-Nagel (Düren, Germany). Standard stock solution of glucose and its corresponding internal standard were prepared in ultrapure water at a concentration of 1000 mg L^{-1} and stored at −20 °C in amber-colored glass vials. A working solution of

glucose at a concentration of 100 mg L^{-1} was prepared by dilution of the stock solution in ultrapure water. Subsequent dilutions of the working solution were made, for the construction of calibration curve and matrix matched samples.

Instrumental analysis

A hydrophilic interaction chromatography (HILIC) method coupled with mass spectrometer triple quadrupole (MS) was performed for the determination of glucose in the samples. Glucose was determined immediately after the completion of sorption experiment. A Thermo TSQ Quantum Access triple quadrupole system (San Jose, CA, USA), equipped with an Electrospray Ionisation Source (ESI), an UHPLC pump (Thermo Accela) and an Accela autosampler was used for the analysis. An Acquity BEH amide chromatographic column (2.1 mm X 100 mm, 1.7 m, Waters Corporation, Milford, MA) was utilized for analytes' determination. The mobile phases were comprised of a mixture of ACN:H$_2$O:NH$_4$OH 89.9:10:0.1% (v:v:v) and (B) ACN:H$_2$O: NH$_4$OH 30:69.9:0.1 (v:v:v). The elution program was isocratic, with a flow rate of 300 μL min^{-1} and the column's temperature was set at 35 °C. The injection volume was set to 10 μL, and each chromatographic run was completed in 8 min. The instrument was operated in negative ionization mode. For data processing, Thermo Fisher Scientific's Xcalibur software, Version 2.3 (Waltham, MA, USA) was employed.

Standard solutions in acetonitrile:H$_2$O 80:20 (v:v) at a concentration of 10 mg L^{-1} for glucose, as well as glucose-^{13}C were prepared. After the direct infusion of these solutions in the ESI, the precursor ion of the analytes and their corresponding product ions, the collision energy (CE), and the tube lens (TL) settings were obtained. Following that, the optimum ESI parameters were ion spray voltage, 3000 V; sheath gas, 30 a.u.; auxiliary gas, 0 a.u.; capillary temperature, 300 °C.

The selected reaction monitoring approach (SRM) was used, and two transitions were selected for obtaining the quantifier and qualifier ion of glucose. Specifically, the quantifier ion (defined as the most abundant ion), and the qualifier ion (defined as the second most intense ion) were picked. Regarding the glucose-^{13}C (IS), the most abundant ion was taken into consideration. The abovementioned parameters are tabulated in the Table S2.

Table S2. Selected reaction monitoring (SRM) transitions of glucose and glucose-[13]C

Analyte		Precursor ion (m/z)	Product ions (m/z) *	Collision energy (eV)	Tube lens	Retention time (min)
Glucose		179	**59**	19	63	4.8
			161	6		
	Internal standard					
Glucose -[13]C (IS)		180	**162**	5	86	4.8

* Where in bold is highlighted the quantification ion
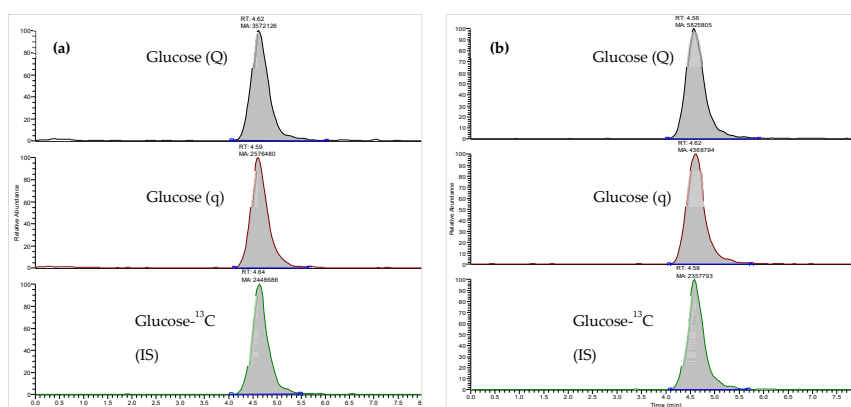
Figure S10. Representative chromatogram of (a) glucose solution (20 mg L^{-1}) used for the absorption (b) the supernatant solution of glucose, using as absorbent the **3D-Fe-MOF** (where glucose (Q) is the quantifier ion of glucose, glucose (q) is the qualifier ion of glucose, and glucose-[13]C (IS) is the most abundant ion for the internal standard (IS).
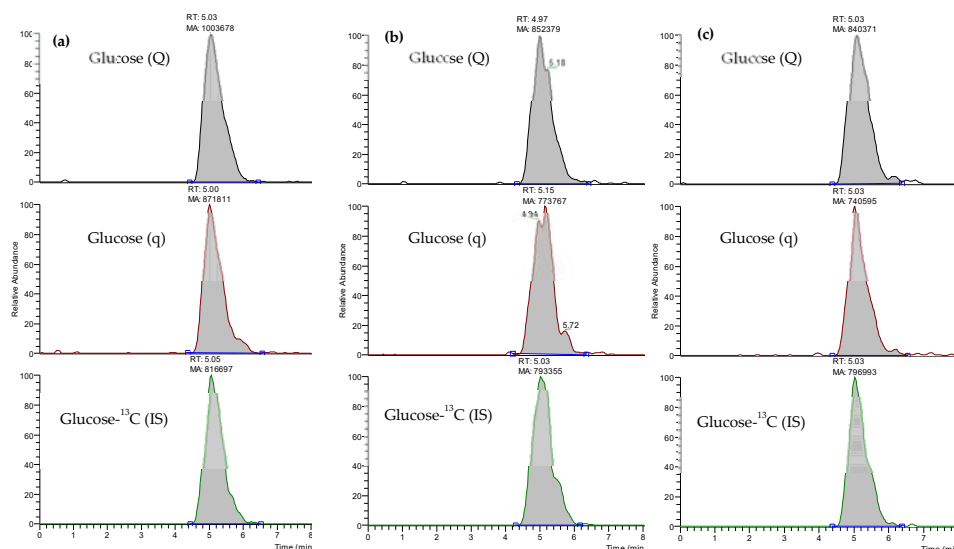
Figure S11. Representative chromatogram of **(a)** glucose standard solution (20 mg L^{-1}) **(b)** glucose solution used for the absorption (20 mg L^{-1}) **(c)** the supernatant solution of artificial sweat using as absorbent the **3D-Fe-MOF** (where glucose (Q) is the quantifier ion of glucose, glucose (q) is the qualifier ion of glucose, and glucose-^{13}C (IS) is the most abundant ion for the internal standard glucose-^{13}C (IS).
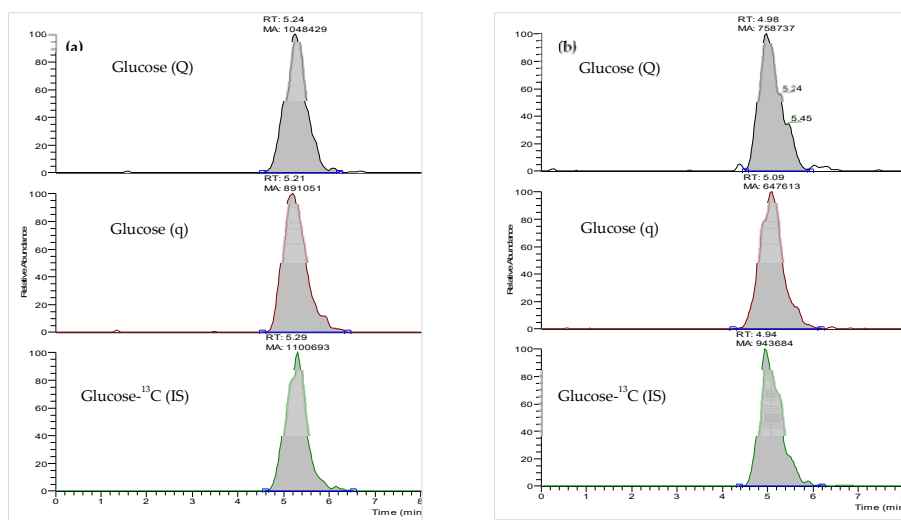

Figure S12. Representative chromatogram of **(a)** standard glucose solution (20 mg L^{-1}) **(b)** supernatant solution of artificial sweat using as absorbent the **2D-Fe-MOF** (where glucose (Q) is the quantifier ion of glucose, glucose (q) is the qualifier ion of glucose, and glucose-^{13}C (IS) is the most abundant ion for the internal standard glucose-^{13}C.

Table S3. Bond Valence Sums (BVS) for the iron atoms in the two structures. (R_o and B values for each calculation. Fe^{II} : R_o = 1.734, B = 0.37, Fe^{III} : R_o = 1.759, B = 0.37).

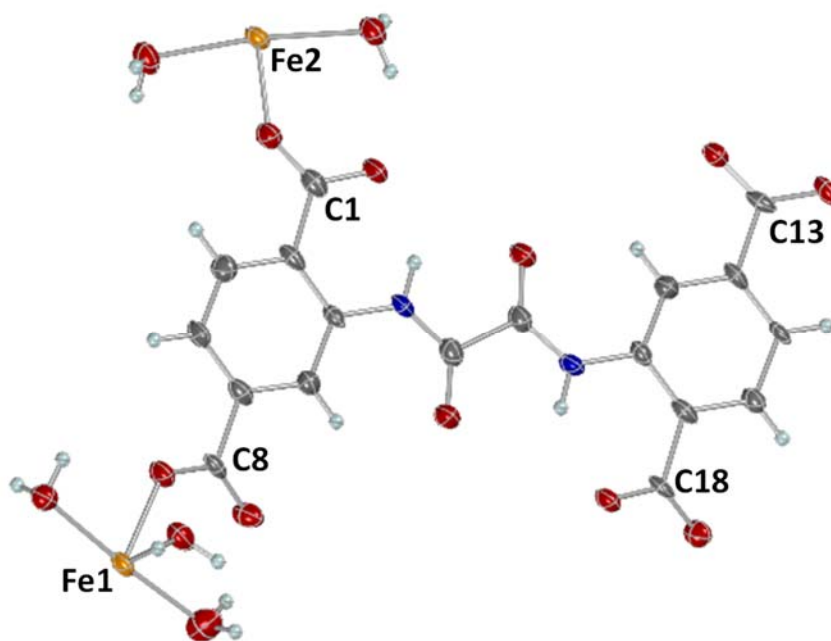| 3D-Fe-MOF				2D-Fe-MOF	
Fe1-O Distances (Å)		**Fe2-O Distances (Å)**		**Fe1-O Distances (Å)**	
Fe1-O8	2.079	**Fe2-O7**	2.177	**Fe1-O1**	2.055
Fe1-O6	2.159	**Fe2-O5**	2.152	**Fe1-O1**	2.055
Fe1-O3	2.060	**Fe2-O11**	2.107	**Fe1-O2**	2.164
Fe1-O2	2.131	**Fe2-O12**	2.137	**Fe1-O2**	2.164
Fe1-O14	2.153	**Fe2-O1**	2.125	**Fe1-O6**	2.179
Fe1-O15	2.219	**Fe2-O13**	2.080	**Fe1-O6**	2.179
BVS (Fe^{II})	2.059	**BVS (Fe^{II})**	2.067	**BVS (Fe^{II})**	2.066
BVS (Fe^{III})	2.203	**BVS (Fe^{III})**	2.211	**BVS (Fe^{III})**	2.211

Figure S13. The asymmetric unit of the **3D-Fe-MOF**. Color code: Fe orange, C, grey, H cyan, O red, N blue.
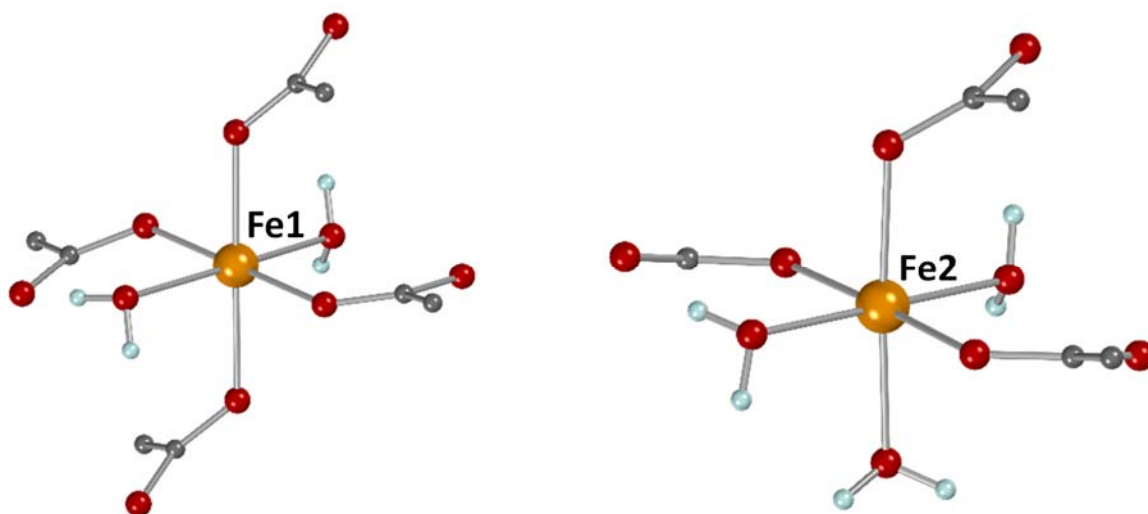
Figure S14. The coordination environment around Fe1 (left) and Fe2 (right) in the crystal structure of the **3D-Fe-MOF**. Color code: same as in Figure S10.
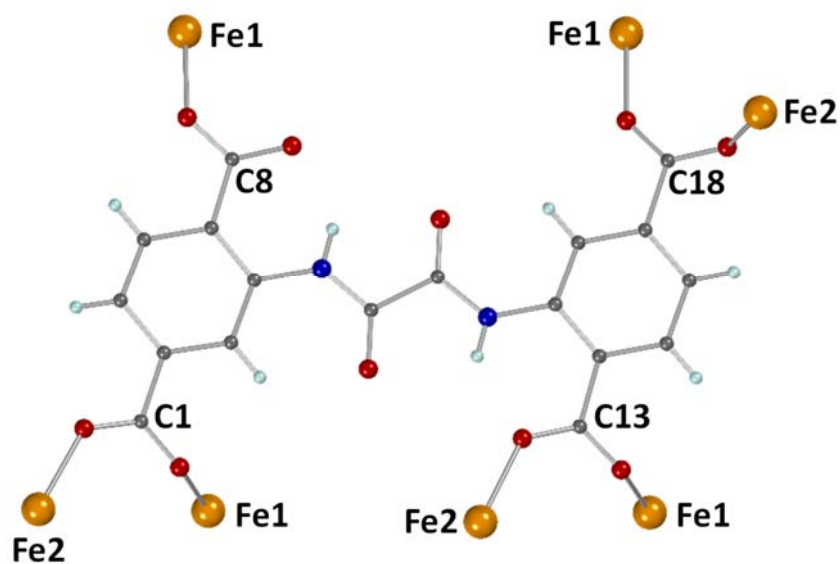

Figure S15. The coordination mode of the tetra-anion of the ligand (H₂L⁴⁻) in the crystal structure of the **3D-Fe-MOF**. Color code: same as in Figure S10.
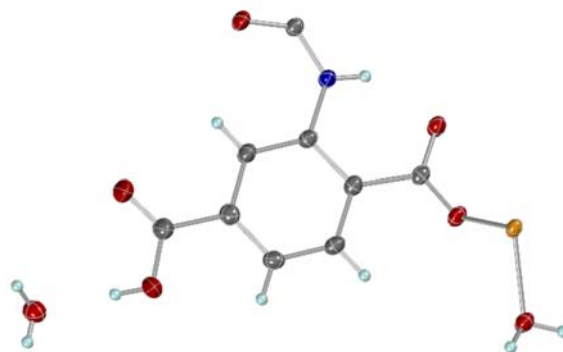
Figure S16. The asymmetric unit of the **2D-Fe-MOF**. Color code: Fe orange, C, grey, H cyan, O red, N blue.
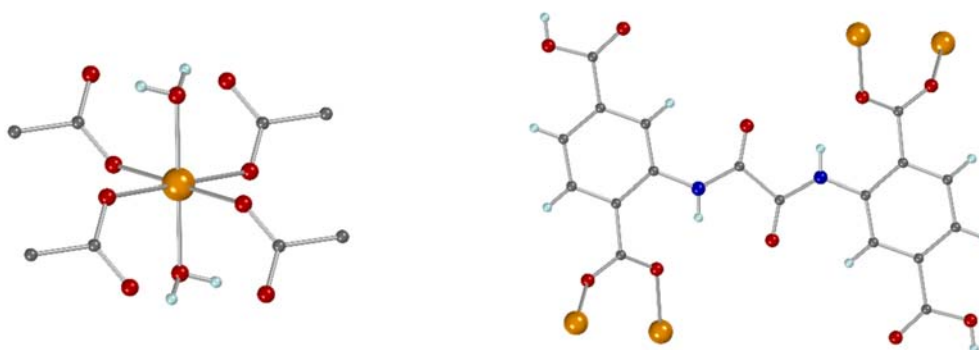

Figure S17. The coordination environment around Fe (left) and the coordination mode of the di-anion of the ligand (H_4L^{2-}) (right) in the crystal structure of the **2D-Fe-MOF**. Color code: same as in Figure S13.
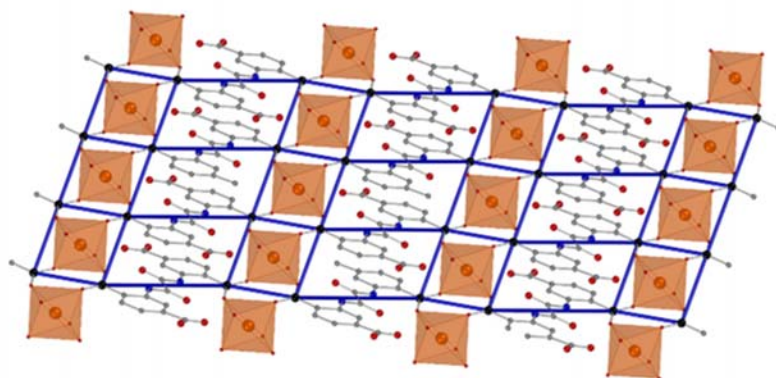
Figure S18. The underline **sql** network of the **2D-Fe-MOF**. Color code: same as in Figure S13.
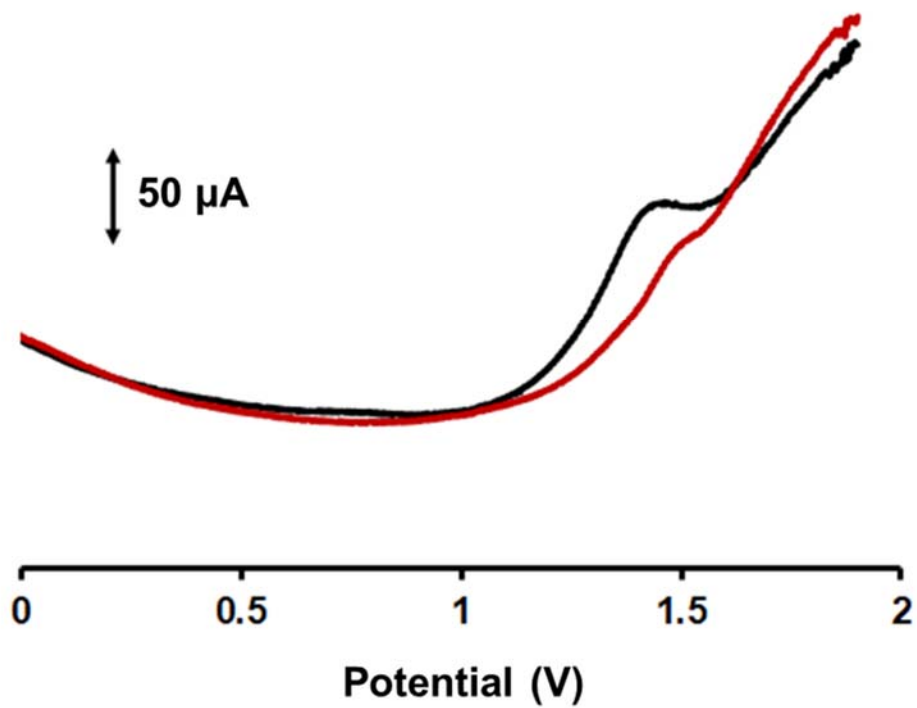

Figure S19. DP voltammograms of 0 and 600 μM GLU at the GPE modified with the **3D-Fe-MOF** in artificial sweat (pH 4.0).